Image Anal Stereol 2024;43:167-183 doi: 10.5566/ias.3039
Original Research Paper

A HISTOGRAM-BASED HEURISTIC FOR AN ADAPTIVE ACTIVE CONTOURS COLOR IMAGE SEGMENTATION

YAMINA BOUTICHE✉,[1], ABDELHAMID ABDESSELAM[2], NAIM RAMOU[1], NABIL CHETIH[1] AND MOHAMMED KHORCHEF[1]

[1]Research Center in Industrial Technologies CRTI, ex CSC P.O.Box 64, Cheraga 16014, Algiers, Algeria,
[2]Department Computer Science, Sultan Qaboos University, Muscat, Oman
e-mail: bouticheyami@gmail.com, y.boutiche@crti.dz, ahamid@squ.edu.om, n.ramou@crti.dz, n.chetih@crti.dz, m.khorchef@crti.dz
(Received September 26, 2023; revised May 28, 2024; accepted May 28, 2024)

ABSTRACT

The fidelity to data (external energy) term in energy-based segmentation of scalar (single channel) images requires setting scalar values defining the weights assigned to the inside and outside energy functional. These values are often determined empirically, which is a tedious and time consuming task. When it comes to color images (multi-channel), the weights become vectors, which further complicates the process of identifying the appropriate weights. In this work, a new interpretation of the weight vector is introduced. It is seen as representing the contribution of each channel in the energy functional, that is equivalent to search an optimum color space. We propose a heuristic formula for estimating the values of the weight vector. It is based on the ratio of the height to the width of the color components histograms. We have applied the proposed formulation to Piecewise Constant Vector Valued (PCVV) model of Chan and Vese in both biphase and multiphase frameworks. Results of the experiments demonstrate the advantages of the proposed model over the commonly used trial and error setting of weights and the model based on color spaces mixing.

Keywords: Active contours, Adaptive weights, Color images, Color spaces, Segmentation.

INTRODUCTION

Human beings have a remarkable ability to analyze and interpret different aspects of the visual information. Color is probably one of the most important features employed by humans to understand the 3D environment (Burger and Burge, 2009). Computer vision systems have also exploited this feature in the analysis of digital images. A wide range of segmentation techniques have been designed to deal with greyscale images. Several of these techniques have been generalized to deal with color images such as thresholding (Nakib *et al.*, 2007; Ng, 2006; Chan *et al.*, 1998), region merging (Zhang *et al.*, 2019; Wang *et al.*, 2016; García-Ugarriza *et al.*, 2008), pixel classification (Vandenbroucke *et al.*, 2003b;a), Active Contours ACs (energy-based or model-based) (Subudhi and Mukhopadhyay, 2021; Lei and Weng, 2021; Brox *et al.*, 2010; Chan *et al.*, 2000) to name a few. We refer the reader to a recent survey of segmentation by color features described in Garcîa-Lamont *et al.* (2018).

When dealing with greyscale images, there is a need to look for the technique that has the best performance for a given application. But working with color images requires defining the technique as well as the adequate color space. In fact, color selection in *RGB* space is difficult and quite non-intuitive. Color selection is more intuitive in other color spaces, since perceptual color features are represented separately. The choice of the color space depends on the application environment. For example, when illumination conditions are not controlled luminance-chrominance color spaces family might be preferred because of the existing separation between the two color properties, luminance and chrominance (Burger and Burge, 2009; Hernández-Hernández *et al.*, 2016). However, further works have been done to get best segmentation performance based on the selection of image's components. Principally, two approaches have been adopted for this purpose: The first one consists of assigning weights to the components of an existing color space. Sought weights are those that lead to the best segmentation. Considering, for example, the *HSI* color space, the optimum space is written as $(\alpha H, \beta S, \gamma I)$. Several ways are done to determine the weights α, β and γ. Moallem *et al.* (2011) proposed $((1/2)H, S, (2/3)I)$ chosen by trial and error while in Mousavi *et al.* (2013) genetic algorithm (GA) is applied to set the weights. The second approach consists of selecting two or more components from two or more color spaces. A dimension reduction method (eg. Principal Component Analysis (PCA)) is then used to select the more significant components, on

which a segmentation will be applied (Dev *et al.*, 2014; Hu *et al.*, 2017).

In the context of ACs segmentation, the estimation of energy functional parameters has a great importance given that the segmentation accuracy is subject to the values attributed to energy weight parameters. Furthermore, such estimation allows to make the use of AC models completely automatic without human interaction. Many ideas have been proposed to deal with this issue (Hu *et al.*, 2017; Li *et al.*, 2018; Hoogi *et al.*, 2017). Our main contribution consists of proposing an automatic estimation of the optimum weights that define the contribution of each color component to the active contour energy functional. The basic idea is to assign a weight that depends on the ability of the channel to discriminate between the foreground and the background. To this end, we propose a heuristic formula based on the color channels' histograms.

In the present work, the proposed heuristic formula is applied to the Piecewise Constant Chan-Vese model for Vector Valued images (PCVV) (Chan *et al.*, 2000). In addition, to overcome the slowness of the standard gradient descent method used in Chan *et al.* (2000), the optimization is done via the sweeping algorithm that was developed for biphase and multiphase level set framework.

The remaining of this paper is arranged as follows. Section 2 introduces the energy functional formulations for graylevel images segmentation and its generalization to color images. Some related works are briefly described in section 3. The proposed model is described in detail in section 4. Experiment results, comparisons and quantitative evaluations are presented and discussed in section 5. Finally, section 6 summarizes this paper.

SEGMENTATION BY ACTIVE CONTOURS

Since the publication of Mumford and Shah (Mumford and Shah, 1989) paper describing segmentation as a variational problem, several models have been derived leading to significant improvements in the image segmentation task. In almost all of implicit active contours, where the curve is represented via level set function, the functional to be optimized is expressed as a summation of three terms as shown in Eq. (1).

1. *A distance regularization term* that ensures the level set is kept as a signed distance function during the evolution process. It is introduced in the energy functional to omit the level set re-initialization step. It is formulated as a simple or a double well-potential function (Li *et al.*, 2005; 2010).
2. *A curve regularization term* that insures the smoothness of the curve during its evolution, thereby avoid the shock phenomena (Mumford and Shah, 1989). It approximates the length term in the energy functional, such it can be utilized to reduce the impact of noise. Many approximations have been proposed, initially, inspired from Tikhonov stabilizers (Kass *et al.*, 1988). Recently, according to Cauchy-Crofton formula and a given neighborhood system, the curve length is approximated by drawing a sufficient number of straight lines with several orientations, varying between angle 0 to 2π, and counting the number of intersections of these lines and the contour (Subudhi and Mukhopadhyay, 2021).
3. *A fidelity to data term* that aims to link the active contour to the image. Different formulations have been used for this term. In Edge-based active contours category, it is expressed using image gradients (Li *et al.*, 2005); in global region-based active contours class, it is expressed as region statistics inside and outside the curve (Chan *et al.*, 2000; Vese and Chan, 2002), and in local region-based active contours category, it is expressed using a kernel function (Gore *et al.*, 2007). A hybrid approach combining local and global image statistics is also considered in several works such as Lei and Weng (2021); Subudhi and Mukhopadhyay (2021); Boutiche and Abdesselam (2017).

$$F^{AC} = \underbrace{\lambda^{in} \underbrace{E^{in}(\Phi,.)}_{\text{Energy inside the curve}} + \lambda^{out} \underbrace{E^{out}(\Phi,.)}_{\text{Energy outside the curve}}}_{\text{Term of fidelity to the data } E_{ext}} + \nu \underbrace{E^{R}(\Phi)}_{\text{Curve regularization}} + \mu \underbrace{E^{DR}(\Phi)}_{\text{Distance regularization}} \quad (1)$$

where E^{out} and E^{in} are energies inside and outside the curve, respectively. λ^{in}, λ^{out}, ν and μ are scalars used to control the contribution of each term in the whole energy functional as follows:

1. ν is the weight of the internal energy term, that penalizes the zero level set functions length. It is formulated as $\nu = \alpha \times 255 \times 255$. Using large values of alpha removes small regions (objects).

Thereby, this weight could be used to improve the segmentation of noised images (He and Osher, 2007).

2.The penalization of distance regularization term is done by the value attributed to the constant μ. Li *et al.* (2010) argued that the model is not sensitive to the choice of μ, and they set it to 0.04.

3.λ^{in}, λ^{out} control the trade-off between the inner and outer energies of the curve. More often the same weight is used by setting $\lambda^{in} = \lambda^{out} = \lambda$. In addition, λ can be used to determine the direction of level set evolution. For λ positive, the level set shrinks inward, while, when it is negative, the level set expends outward (Mumford and Shah, 1989).

To fit color images, the fidelity to data term in Eq. (1) is rewritten as a summation of the color components energies as shown in Eq. (2).

$$E^{ext} = \frac{1}{N}\left[\sum_i^N \lambda_i^{in} E_i^{in} + \sum_i^N \lambda_i^{out} E_i^{out}\right], \qquad (2)$$

where N represents the number of image components. Here, the constant λ becomes a constant vector $(\lambda_1, \lambda_2, \ldots, \lambda_N)$.

Previous ACs usually set error term weights λ_i^{in} and λ_i^{out} arbitrary, more often they are set to the vector $[1, 1, 1]$ (Vese and Chan, 2002). Because this setting does not suit all images, several works have been proposed to automatically estimate λ. In Li *et al.* (2018), λ is treated as the weight of the corresponding sub-domain Ω_k, and it is estimated as the ratio of the surface of Ω_k to the surface of the whole image's domain Ω. In Hu *et al.* (2017) the weight is estimated based on the contrast between the object and the background. In this work, we propose to link the computation of λ to the corresponding component histogram. Therefore, the value of each element in the vector $\lambda = (\lambda_1, \lambda_2, \ldots, \lambda_N)$ determines how much the corresponding component affects the energy of AC. This leads to an optimum color space construction. The following notations will be adopted in the remainder of this paper.

Table 1. *Notation used in the paper*

Notation	Explication
u_0	original grey-scale (single-channel) image
$u_{0,i}$	original color (multi-channel) image
Ω	domain of image definition
$\mathbf{x} = (x, y)$	represents the pixel coordinates.
H_ε	the regularized Heaviside function
δ_ε	Heaviside derivative
$i = 1, \ldots N$	used to sweep image's channels
$k = 1, \ldots, K$	used to sweep image's sub-domains obtained by bi-phase or multi-phase level sets

RELATED WORKS

In this section, we briefly review some works related to the proposed method, including the Piecewise Constant Chan-Vese for Vector-Valued images (PCVV) model for biphase and multiphase framework (Chan *et al.*, 2000; Vese and Chan, 2002), Principal Component Analysis (PCA)-based Multicomponent selection C-V model (*PMCV*) (Hu *et al.*, 2017) and an Adaptive Energy Weight Based Active Contour Model (Li *et al.*, 2018).

PIECEWISE CONSTANT CHAN-VESE FOR VECTOR-VALUED IMAGES

The Bi-phase Piecewise Constant Chan-Vese for Vector-Valued images (B-PCVV) model is formulated to approximate a given image $u_{0,i}$ by two constants that represents the intensity means inside and outside the curve (c^{in} and c^{out}) respectively. Thereby it is used for single-object segmentation. The level set evolution of B-PCVV model (Vese and Chan, 2002) is achieved by minimizing the following energy functional.

$$\begin{aligned} F(c^+, c^-, \Phi) = \mu \int_\Omega \delta_\varepsilon(\Phi(\mathbf{x}))|\nabla\Phi(\mathbf{x})|\,\mathbf{dx} \\ + \frac{1}{N}\int_\Omega \sum_i^N \lambda_i^{in}\left(u_{0,i}(\mathbf{x}) - c_i^{in}\right)^2 \\ \times \mathrm{H}_\varepsilon(\Phi)\,\mathbf{dx} \\ + \frac{1}{N}\int_\Omega \sum_i^N \lambda_i^{out}\left|u_{0,i}(\mathbf{x}) - c_i^{out}\right|^2 \\ \times (1 - \mathrm{H}_\varepsilon(\Phi))\,\mathbf{dx}, \\ i = 1, \ldots N. \end{aligned} \qquad (3)$$

$c^{in}(\Phi)$ and $c^{out}(\Phi)$ are the constant vectors that compute the means inside and outside the curve in each

image components. They are defined as follows:

$$c_i^{in}(\Phi) = \frac{\int_\Omega u_{0,i}\, \mathrm{H}_\varepsilon(\Phi)\mathbf{dx}}{\int_\Omega \mathrm{H}_\varepsilon(\Phi)\, \mathbf{dx}}, \qquad c_i^{out}(\Phi) = \frac{\int_\Omega u_{0,i}\, \big(1-\mathrm{H}_\varepsilon(\Phi)\big)\mathbf{dx}}{\int_\Omega \big(1-\mathrm{H}_\varepsilon(\Phi)\big)\, \mathbf{dx}} \tag{4}$$

The optimum of the functional in Eq. (3) is obtained by solving the following gradient descent flow (Vese and Chan, 2002):

$$\frac{\delta\Phi}{\delta t} = \delta_\varepsilon \left[\mu\ \mathrm{div}\ \left(\frac{\nabla\Phi}{|\nabla\Phi|}\right) - \frac{1}{N}\sum_i^N \lambda_i^{in}\left(u_{0,i}(\mathbf{x}) - c_i^{in}\right)^2 + \frac{1}{N}\sum_i^N \lambda_i^{out}\left(u_{0,i}(\mathbf{x}) - c_i^{out}\right)^2\right] \tag{5}$$

Vese and Chan proposed Multi-phase Piecewise Constant Chan-Vese for Vector-Valued images (M-PCVV) (Vese and Chan, 2002), which is a generalization of biphase case. It is used to extract 2^n targets with n level set functions. Considering the case of two level set functions ($n = 2$) Φ_1 and Φ_2, thus the image's domain Ω is sub-divided to four sub-domains $k = 1 \ldots 4$ as

$$\begin{cases} \Omega_1 \text{ if } \mathbf{x} \in (\Phi_1(\mathbf{x}) > 0 \text{ and } \Phi_2(\mathbf{x}) > 0); \\ \Omega_2 \text{ if } \mathbf{x} \in (\Phi_1(\mathbf{x}) > 0 \text{ and } \Phi_2(\mathbf{x}) < 0); \\ \Omega_3 \text{ if } \mathbf{x} \in (\Phi_1(\mathbf{x}) < 0 \text{ and } \Phi_2(\mathbf{x}) > 0); \\ \Omega_4 \text{ if } \mathbf{x} \in (\Phi_1(\mathbf{x}) < 0 \text{ and } \Phi_2(\mathbf{x}) < 0). \end{cases} \tag{6}$$

The external energy on Chan-Vese model to fit victor-valued images is formulated as shown in Eq. (7) (Chan *et al.*, 2000)

$$\begin{aligned} E_{\text{ext}}(\Phi_1,\Phi_2,c_i) \quad &= \frac{1}{N}\int_{\Omega_1}\sum_i^N \lambda_i \left|u_{0,i}(\mathbf{x}) - c_i^1\right|^2 \mathbf{dx} \\ &+ \frac{1}{N}\int_{\Omega_2}\sum_i^N \lambda_i \left|u_{0,i}(\mathbf{x}) - c_i^2\right|^2 \mathbf{dx} \\ &+ \frac{1}{N}\int_{\Omega_3}\sum_i^N \lambda_i \left|u_{0,i}(\mathbf{x}) - c_i^3\right|^2 \mathbf{dx} \\ &+ \frac{1}{N}\int_{\Omega_4}\sum_i^N \lambda_i \left|u_{0,i}(\mathbf{x}) - c_i^4\right|^2 \mathbf{dx} \end{aligned} \tag{7}$$

The four constant vectors of average pixel values for each sub-domain are calculated as shown in Eq. (8)

$$c_i^1 = \frac{\int_{\Omega_1} u_{0,i}(\mathbf{x})\,\mathbf{dx}}{m_1}, \quad c_i^2 = \frac{\int_{\Omega_2} u_{0,i}(\mathbf{x})\,\mathbf{dx}}{m_2}, \quad c_i^3 = \frac{\int_{\Omega_3} u_{0,i}(\mathbf{x})\,\mathbf{dx}}{m_3}, \quad c_i^4 = \frac{\int_{\Omega_4} u_{0,i}(\mathbf{x})\,\mathbf{dx}}{m_4}, \tag{8}$$

where the m_1, m_2,m_3 and m_4 denote the surface of the sub-domains Ω_1, Ω_2, Ω_3 and Ω_4, respectively.

In Chan *et al.* (2000) the level set evolution is achieved by the iterative process of gradient descent as $\Phi^{n+1} = \Phi^n + \triangle t\, \frac{\delta\Phi}{\delta t}$. The time step $\triangle t$ has to obey the Courant-Friedrichs-Lewy condition for numerical stability, thus it is set to a small value. In both above models (B-PCVV and M-PCVV) the parameters are set empirically, most of the time $\lambda_{in} = \lambda_{out} = 1$ when u_0 is a scalar intensity image (single-channel) image and to $\lambda_{in} = \lambda_{out} = [1,1,1]$ when $u_{0,i}$ is a victor-valued (three-channel) image. Furthermore, to the best of our knowledge, Chan-Vese models are tested and evaluated on RGB color space only.

PRINCIPAL COMPONENT ANALYSIS (PCA)-BASED MULTICOMPONENT SELECTION C-V MODEL (*PMCV*)

Hu et all in Hu *et al.* (2017), proposed a method called Principal Component Analysis-based Multicomponent selection C-V model (*PMCV*). The idea consists of applying PCA method to *RGB* and *HSV* color space components and select three PCA-transformed components. A k-means algorithm ($k = 2$) is then applied to each selected PCA-component to obtain foreground/background segmentation. K-means algorithm is used as pre-segmentation from which adaptive weights are calculated using the formulas shown in Eqs. (9) and (10).

$$k_t(i) = \frac{|k_{qj}(i) - k_{bj}(i)|}{\max(k_{qj}(i), k_{bj}(i))} \tag{9}$$

$$k_t(i) = \frac{k_t(i)}{\sum_{i=1}^3 k_t(i)} \quad i = 1,2,3, \tag{10}$$

where $k_t(i)$ represents the weight of the i^{th} component, $|.|$ is the absolute value, $k_{qj}(i)$ and $k_{bj}(i)$ are the mean of foreground and background pixel values of the i-th component respectively. In addition, the cluster centers of the k-means clusters $A^{(i)}$ are regarded as the mean of Ω_{in} . Thereby, the modified energy functional of C-V model is done by:

$$E(\Phi,A^{(i)},c_2) = \mu \int_{\Omega} \delta_{\varepsilon}(\Phi)\nabla\Phi \,\mathbf{dx} + \int_{\Omega_{in}} \sum_{i=1}^{3} \left[k_t(i) \left(u_0^{(i)}(\mathbf{x}) - A^{(i)} \right)^2 \right] \times \mathrm{H}_{\varepsilon}(\Phi)\,\mathbf{dx} + \int_{\Omega_{out}} \sum_{i=1}^{3} \left[k_t(i) \left(u_0^{(i)}(\mathbf{x}) - c_2^{(i)} \right)^2 \right] \times (1-\mathrm{H}_{\varepsilon}(\Phi))\,\mathbf{dx} \tag{11}$$

The numerical implementation of the model was done using the implicit finite difference schema as in (Chan *et al.*, 2000) and the optimization of the functional defined by Eq. (11) was performed via the gradient descent method, with $\Phi^{n+1} = \triangle t\, F_{PMCV} + \Phi^n$, using an adaptive iteration termination criterion. The PMCV method was applied to extract wheat leaf lesion from color images. It was tested on 55 wheat leaf images taken over 29 days from April 14, 2014 to May 12, 2014. The authors reported an accuracy of 84.17% for PMCV against 65.79% for B-PCVV method. However, the evaluation was done only in the bi-phase level set framework.

ADAPTIVE ENERGY WEIGHT BASED ACTIVE CONTOUR MODEL

Recently, Li *et al.* (2018) introduced a general formulation to compute fidelity data term parameters, where the magnitude of the energy terms $E^{in}(\Phi,.)$ and $E^{out}(\Phi,.)$ are positively correlated with the number of pixels (area) associated to corresponding region (Ω_{in} and Ω_{out}). The weight parameters are set as shown in Eq. (12) for the bi-phase level set framework and Eq. (13) for multiphase framework.

$$\begin{aligned} \lambda_{in}^n &= f_1(\Phi^n) = \frac{\int_{\Omega}(1-H(\Phi^n))\mathbf{dx}}{N_x N_y} \\ \lambda_{out}^n &= f_2(\Phi^n) = \frac{\int_{\Omega} H(\Phi^n)\mathbf{dx}}{N_x N_y} \end{aligned} \tag{12}$$

$$\lambda_k^n = f(\Phi_1^n,\Phi_2^n) = \frac{N_x N_y}{area(\Omega_i)}, \quad k = 1\ldots 4\ , \tag{13}$$

where n denote the n^{th} iteration, N_x and N_y are length and width of the image. $H(\Phi^n)$ used to delimit the inside curve and $(1-H(\Phi^n)$ for outside curve. For a robust and fast convergence of the level set functions, authors proposed first a coarse segmentation using fuzzy k-means clustering method. The final segmentation is achieved by solving the PDEs of Chan-Vese model. During the iterative process, the energy weight parameters λ_{in}^n and λ_{out}^n are updated adaptively by Eqs. (12) and (13) in biphase and multiphase cases, respectively. The performance evaluation is carried on grayscale synthetic and general medical images (CT, ultrasound, MR and PET). The average segmentation errors is 6.83% against 9.45% for classic Chan-Vese model initialized with threshold method.

PROPOSED APPROACH

Histograms are often used to determine if an image is making effective use of its intensity range by examining the size and uniformity of the histogram's distribution (Burger and Burge, 2009). The main idea of the proposed formulation came from the visualization of the components' histograms for different color spaces. We noticed that the components that correspond to the chroma information in the color spaces often show a lopsided shape with narrow dynamic range. On the other hand, the histogram of luminance component usually exhibits relatively flat shape with large dynamic range. In other words, the dynamic range of the chroma channels is smaller than that of the luminance channel. This is confirmed by the obtained ranges of gray level variation on three different datasets "Oxford flowers", "Butterfly" and *CUB_200_2011*, summarized in Table 2. In addition, an example of the image "flowers" in Figs. 1 displayed in five different color spaces (*RGB*, $L^*a^*b^*$, *HSV*, YC_rC_b, and $I_1I_2I_3$). For each color space, the top row shows images of the three channels and the bottom row the corresponding histograms.
From the Table 2 and Fig. 1, it is observed that in the RGB color space the dynamic ranges is large for the three channels because of the luminance information is embedded in the three components.
However, in the other color spaces the histogram of the chroma components present a less range of gray level variations. The smaller ranges are observed in the YC_rC_b and $I_1I_2I_3$.

Based on this observation, we devised the heuristic formulas shown in Eq. (14) and Eq. (15).

$$\begin{cases} h_i = & \max(H_i) - \min(H_i), \\ w_i = & \max(W_i) - \min(W_i), \ i = 1\ldots N \end{cases}\ , \tag{14}$$

where H_i is the histogram of the i-th component and W_i represents the dynamic range of the image component i. Then a ratio between the high and the width is computed as follows:

$$\lambda_i = \frac{h_i}{1+w_i} \tag{15}$$

To the best of our knowledge, the role of the weight λ is limited to adjust the external energy. However, if we

Table 2. *The mean variation ranges of each component (Comp.) in different color spaces computed on the three datasets*

Datasets (number of images)	color spaces	Comp.1	Comp.2	Comp.3
Oxford flowers (355)	*RGB*	154.53	165.45	104.35
	$L^*a^*b^*$	126.78	53.22	77.56
	HSV	47.37	101.55	160.86
	YC_rC_b	164.88	39.74	26.89
	$I_1I_2I_3$	134.99	37.95	30.91
Butterfly (832)	*RGB*	131.71	148.75	100.73
	$L^*a^*b^*$	113.33	47.18	61.44
	HSV	42.79	94.33	133.20
	YC_rC_b	150.51	33.46	25.06
	$I_1I_2I_3$	119.64	29.60	24.32
*CUB*_200_2011 (60)	*RGB*	97.57	95.51	97.92
	$L^*a^*b^*$	73.42	15.13	21.33
	HSV	14.82	51.73	96.70
	YC_rC_b	100.67	12.90	13.82
	$I_1I_2I_3$	82.70	15.71	6.52

look at it from another angle, we can see that it controls the contribution of each image component in the active contour energy. To detail this, we rewrite the first term of the Eq. 2 in its developed form as:

$$E_{ext}^{in} = \frac{1}{N}\sum_{i}^{N} \lambda_i (u_{0,i} - u)^2, \tag{16}$$

where u presents an approximation of the original image $u_{0,i}$. After development we find

$$\begin{aligned} E_{ext}^{in} = \frac{1}{N}[\lambda_1 u_{0,1}^2 + \lambda_2 u_{0,2}^2 + \lambda_3 u_{0,3}^2 - \lambda_1 u_{0,1} u - \\ \lambda_2 u_{0,2} u - \lambda_3 u_{0,3} u + \lambda_1 u^2 + \lambda_2 u^2 + \lambda_3 u^2] \end{aligned} \tag{17}$$

It is clear from (17), that the values of the vector components λ control the contribution of each image component in the fidelity to data term. The proposed formula (Eq.(15)) allows to give more weight to the component that discriminates better the foreground/background in the image to be segmented.

AUTOMATIC WEIGHT SETTING IN THE PCVV MODEL WITH FAST OPTIMIZATION ALGORITHM

In this section, we describe the modifications we introduced to the implementation of the famous Piecewise Constant for Vector Valued (PCVV) Chan-Vese model (Vese and Chan, 2002) in both biphase and multi-phase frameworks.

Biphase framework

In the classic PCVV, the vector λ is set empirically, thereby the segmentation accuracy is significantly affected and human interaction is needed. We have noticed that the values assigned to λ have a greater influence on the segmentation accuracy in the color spaces other than the RGB space. To deal with this limitation, we apply the automatic calculation of the weights described in section 4. This has the advantage to calculate the wights automatically according to the processed image and the considered color space. Moreover, to remedy the slow convergence of the gradient descent algorithm, we have adopted a fast optimization algorithm based on sweeping principle described in Song and Chan (2002); Boutiche and Abdesselam (2017). In this algorithm, the energy is re-evaluated whenever a point $\mathbf{x}$ moves from inside a curve to outside ($\triangle F_{12}$) and vice versa ($\triangle F_{21}$) as described in Eq. (18), and Eq. (19).

$$\begin{aligned} \triangle F_{12} = \frac{1}{N}\Big[\sum_i^N \lambda_i \left(u_{0,i}(\mathbf{x}) - c_i^{out}\right)^2 \frac{n}{n+1} \\ - \sum_i^N \lambda_i \left(u_{0,i}(\mathbf{x}) - c_i^{in}\right)^2 \frac{m}{m-1}\Big] \end{aligned} \tag{18}$$

$$\begin{aligned} \triangle F_{21} = \frac{1}{N}\Big[\sum_i^N \lambda_i \left(u_{0,i}(\mathbf{x}) - c_i^{in}\right)^2 \frac{m}{m+1} \\ - \sum_i^N \lambda_i \left(u_{0,i}(\mathbf{x}) - c_i^{out}\right)^2 \frac{n}{n-1}\Big], \end{aligned} \tag{19}$$

where n and m represent the number of pixels outside and inside the curve respectively. In this

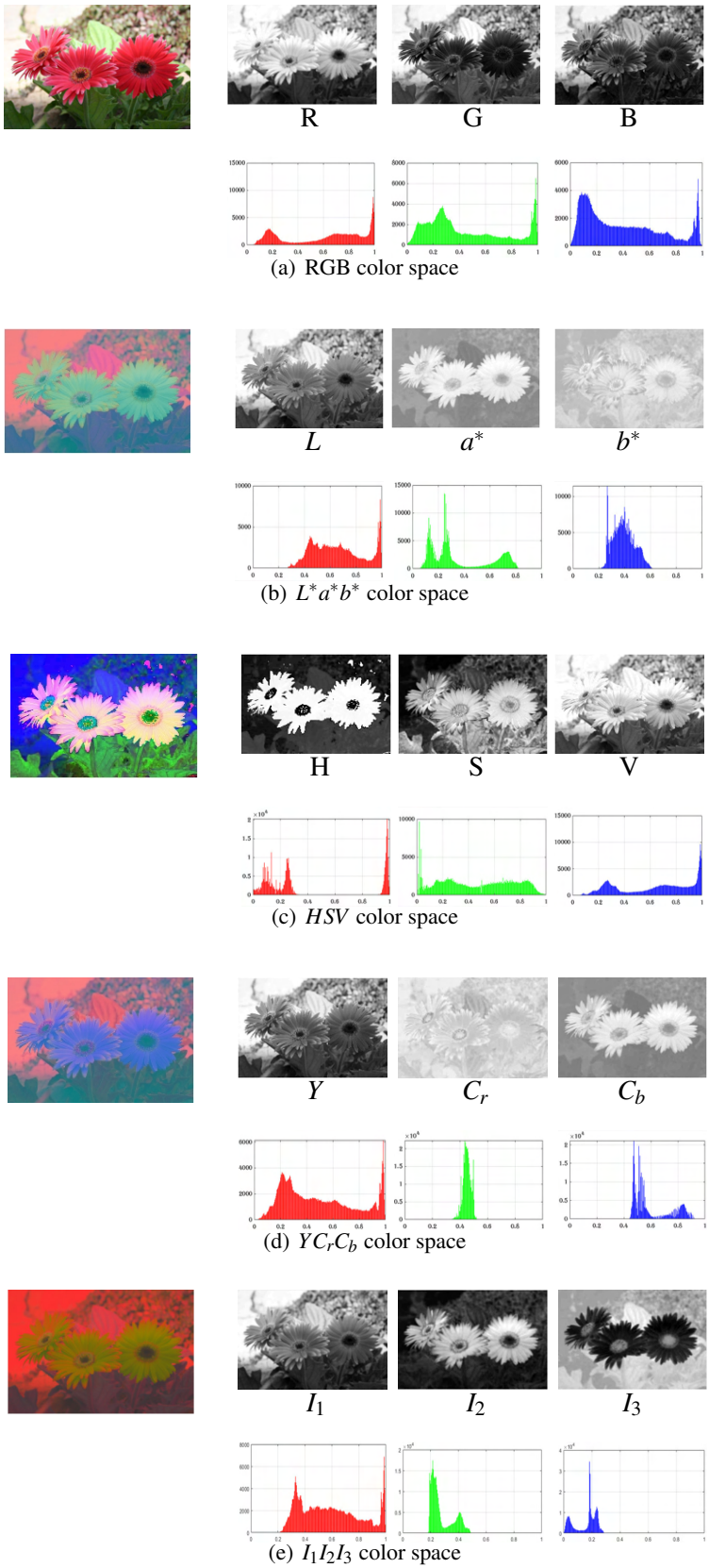

Fig. 1. *Example of an image in different color spaces and the associated individual components with histograms. It shows that the histogram that corresponds to luminance (L^*, V, Y, I_1) component has large dynamic range compared to color components.*

implementation, we have assigned the same weight ($\lambda_i^{in} = \lambda_i^{out} = \lambda_i$) to the inside and outside energies.

Multiphase framework

In the multiphase framework, we have considered the case of two level set functions Φ_1 and Φ_2. It can be generalized easily to more than two level set functions. In the same way, we adopted the optimization via sweeping principal for multiphase level set introduced in He and Osher (2007), and we generalized it to fit vector-valued images. The algorithm checks whether the energy decreases or not when a point $\mathbf{x}$ moves to another sub-domain. The energy variation is computed each time a pixel is moved to another sub-domain. Denote by $\triangle(F_{1-2})$ the energy variation occurring when a pixel is moved from Ω_1 to Ω_2. The new sizes of the subdomains Ω_1 and Ω_2 become $|\Omega_1| - 1$ and $|\Omega_2| + 1$, respectively.

$$\begin{aligned}\triangle F_{(1-2)} = \quad & \frac{1}{N}\left[-\frac{m_1}{m_1-1}\sum_i^N \lambda_i \left(u_{0,i}(\mathbf{x}) - c_i^1\right)^2 \right. \\ & \left. + \frac{m_2}{m_2+1}\sum_i^N \lambda_i \left(u_{0,i}(\mathbf{x}) - c_i^2\right)^2\right]\end{aligned} \tag{20}$$

where c_i^2 and c_i^2 represent the mean intensities of sub-domains Ω_1 and Ω_2, respectively. They are computed using Eq. (8).

EXPERIMENTAL RESULTS AND EVALUATIONS

In this section we describe the various experiments we have conducted. The first two experiments were designed to evaluate the robustness of the proposed automatic weight setting method to noise and to the initial setting of the curve. The subsequent experiments were designed to evaluate the add-value to the B-PCVV (Chan *et al.*, 2000) of the proposed method and compare its performance against another automatic weight setting method PMCV (Hu *et al.*, 2017). Two types of evaluations have been considered, a qualitative evaluation based on the visual inspection of the resulting segmentation and a quantitative evaluation based on the estimation of the segmentation accuracy and the method efficiency in terms of execution time and number of iterations. The accuracy of the segmentation is estimated using the formula in Eq. (21).

$$ACC = \frac{|I_f \cap I_b|}{|I_f \cup I_b|} \times 100\% \tag{21}$$

where I_f denotes the foreground pixels returned by the algorithm and I_b denotes the foreground pixels in the ground truth image and $|x|$ denotes the cardinality of the set x. ACC values are in the range $[0\% - 100\%]$. Moreover 630 images and 5 common color spaces (*RGB*, $L^*a^*b^*$, $I_1I_2I_3$, *HSV* and YC_rC_b) were considered in the performance evaluation experiments. The implementation of variational level sets context, where the optimization is done via gradient decent requires setting several parameters: μ, α, $\triangle t$, ε and in some cases r the width of narrowband and the optimal values depend on the image to be segmented (Hu *et al.*, 2017). On the contrary, the sweeping algorithm we have applied does not require any parameter setting and is not sensitive to the level set initialization as demonstrated in the experiment 5.2 and also reported in Boutiche and Abdesselam (2017). Therefore, for all the experiments, where initial contour isn't shown, the level set function Φ_0 is set to a rectangle binary function ($\Phi_0 = +1$ inside and $\Phi_0 = -1$ outside). In order to exclude possible noisy pixels and also prevent having the minimum of (h_i) equal to 0, we removed bins having less than 10% of maximum (h_i) before applying equation (15) to calculate λ. All the experiments are conducted on Intel(R) Core(TM) i7, with CPU 3:40GHz and 10 GB RAM, under windows 10. Matlab2018 is used to implement the models our model and those compared to.

ROBUSTNESS TO NOISE

Fig. 2 shows the segmentation results of the model for two images corrupted by different levels of noise. The first image represents a dark airplane on light sky and the second image represents a light flower on a dark background. The corruption is obtained by adding a mixture of "Gaussian", "salt & pepper" and "speckle" noises. The PSNR is used to quantify the degree of corruption and is displayed for each image in Fig. 2. The results in Fig. 2 show that, in all cases, the initial contour converges successfully to the object boundaries. In addition, the evaluation of segmentation performance in Table 3 indicates that, up to $PSNR = 31dB$, the segmentation accuracy is slightly and gradually affected by the increasing noise level. These results confirm the noise robustness of the proposed method. However, if the corruption degree is higher then $31\,dB$, a pre-processing step is needed to obtain a better segmentation of the image.

Table 3. *Segmentation accuracy Acc(%) of all degradation degrees in Fig.2*

Airplane	(a)	(c)	(e)	(g)	(i)
	98.41	98.41	98.39	98.32	98.08
Flower	(b)	(d)	(f)	(h)	(j)
	99.36	99.36	99.28	99.13	99.01

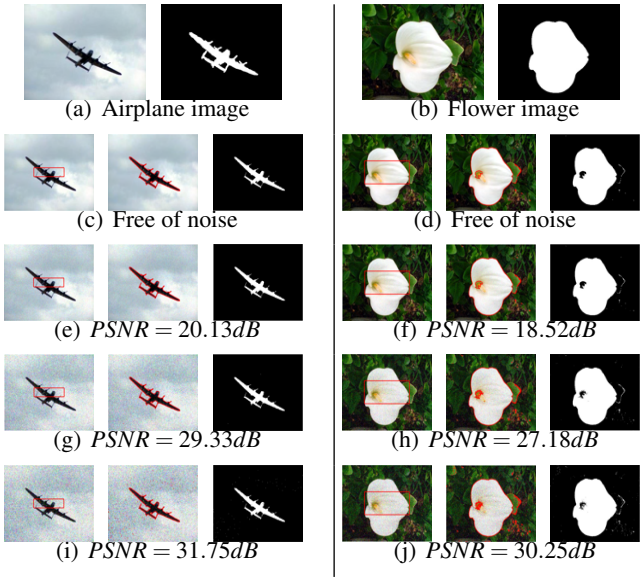

Fig. 2. *Testing of the sensitivity to noise on airplane and flower images. The first row: the original images and their ground truth. The* 2^{nd} *to* 5^th *rows obtained segmentation on different corruption degree, represent as initial contour (red line), converged zero-level set (red line) and the binary mask of the segmentation result.*

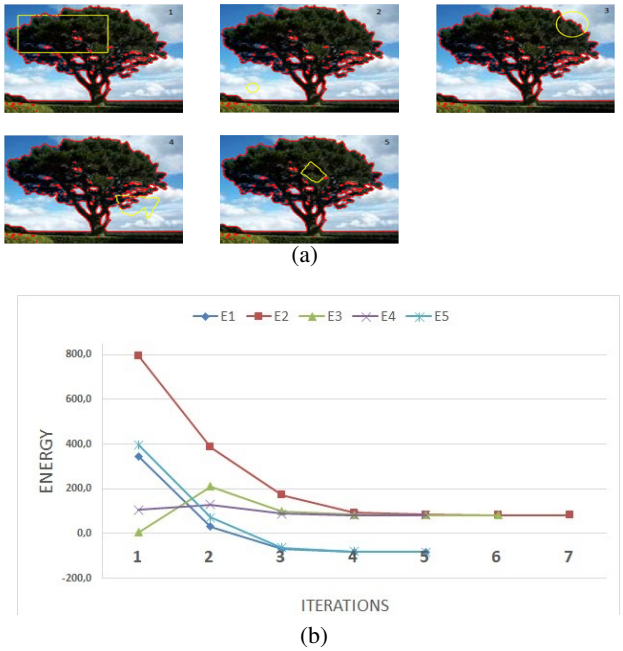

Fig. 3. *Segmentation results with different initial contours. (a) tree image with initial curve (yallow line) and converged curve (red line). (b) The functional energy variations for each initialization in (a).*

ROBUSTNESS TO INITIALIZATION

To demonstrate the robustness of the proposed method to contour initialization, we considered several shapes and locations of the initial contour, see Fig. 3. The model is capable of segmenting the image under different initializations, where in all cases the initial curve converges to the same location (object boundaries) as shown in Fig. 3(a)). However, the convergence time and the energy variation are affected by the initialization (see Fig. 3(b)). The convergence is achieved in just 5 iterations for the initialization in the cases 1, 4 and 5, while, in the cases 2 and 3 the number of iterations are 6 and 7, respectively.

PERFORMANCE AND EVALUATION IN BI-PHASE FRAMEWORK

We have conducted two types of performance evaluation. A qualitative evaluation based on the visual inspection of the segmentation results and a quantitative evaluation based on the estimation of the segmentation accuracy using Eq. (21).

Qualitative Evaluation on Bi-phase Case

We applied the three methods: (PCVV (with λ set to $[1,1,1]$), PMCV) discussed in section 3, and the proposed method (with automatic calculation of λ vector) introduced in section 4 to a set of images (horse, flower and bird) characterized by a complex background and different illumination conditions (presence of shadow and strong uneven illumination).

In Figs. 4, 5 and 6 illustrate the segmentation results obtained on the three images respectively. The original image is displayed on top of each Fig. the following 4 rows show the segmentation results obtained by PCVV and the proposed method on the four color spaces (RGB, $L^*a^*b^*$, $I_1I_2I_3$, HSV and YC_rC_b) respectively. The white lines in the first and third column indicate the zero level set convergence obtained by PMCV and the proposed method while the second and fourth column show the resulting segmentations. The last row shows the zero level set convergence and the resulting segmentation produced by PMCV.

We can see that the proposed method produces a better segmentation than PCVV and PMCV, especially when images present challenging illumination conditions (Figs.5 and 6), where for each case the object is correctly extracted from the background.

The superiority of the proposed method resides on its capability to adjust the contribution of each image's component in the whole energy functional. The contribution of the luminance component is minimized by a small λ_k compared to the chroma components. This is well shown on the Table 4, that summarizes the obtained vector values λ_k in each color space. Each component that corresponds to the luminance/brightness component (L^*, I_1, V, Y for

$L^*a^*b^*$, $I_1I_2I_3$, *HSV* and YC_rC_b respectively) get very low (close to zero) weight. However, this is not the case for the *RGB* color space because the luminance is mixed with the chroma information. This may explain the similar performance of all methods in *RGB* color space. *PMCV* model gives a high quality segmentation result on the horse image, but it fails to do the same on the flower and bird images. PCA components are results from a combination of the channels including those carrying the luminance information.

Horse image

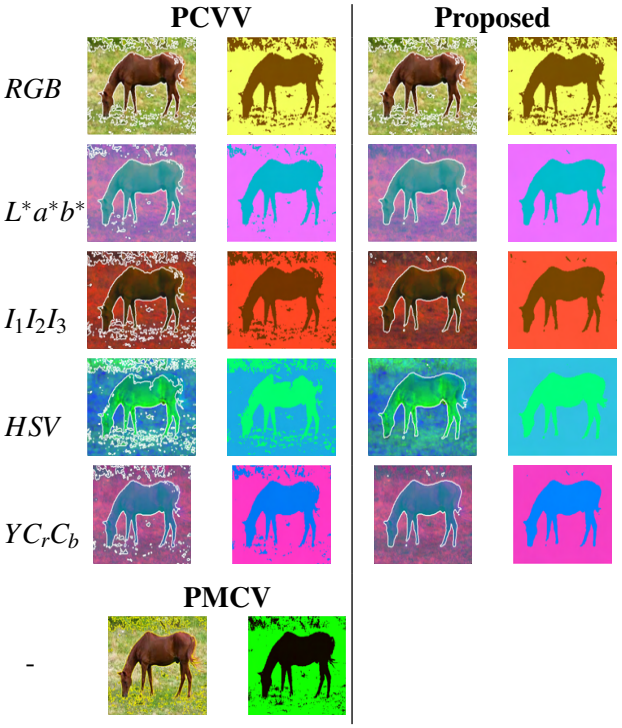

Fig. 4. *Segmentation results of the horse image in most used color spaces. Columns 2 and 3 show the converged zero level set function and corresponding segmented image by classic B-PCVV model with* $\lambda = [1, 1, 1]$*, respectively. Columns 4 and 5 show the results by the proposed improved B-PCVV model. The last row shows the result of the PMCV model.*

Flower image

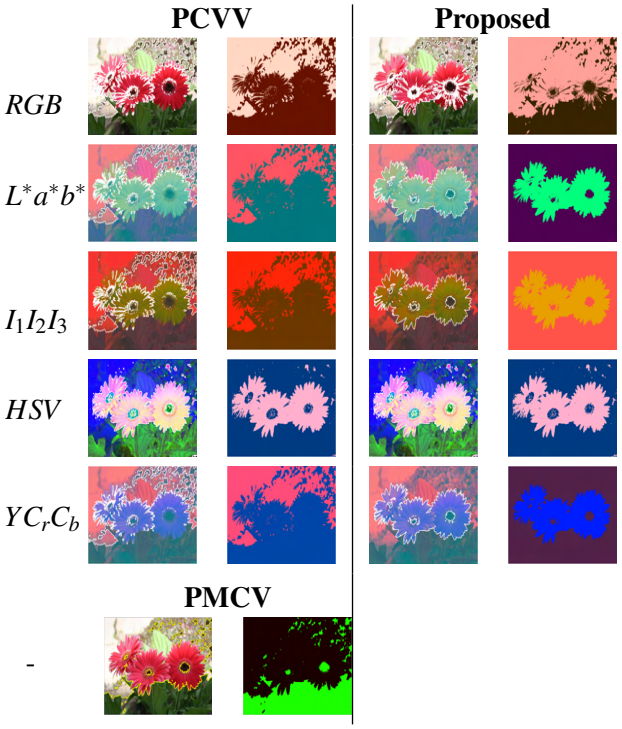

Fig. 5. *Segmentation results of the flower image in commonly used color spaces. Columns 2 and 3 show the converged zero level set function and corresponding segmented image by classic B-PCVV model with* $\lambda = [1, 1, 1]$*, respectively. Columns 4 and 5 show the results by the proposed improved B-PCVV model. The last row shows the result of the PMCV model.*

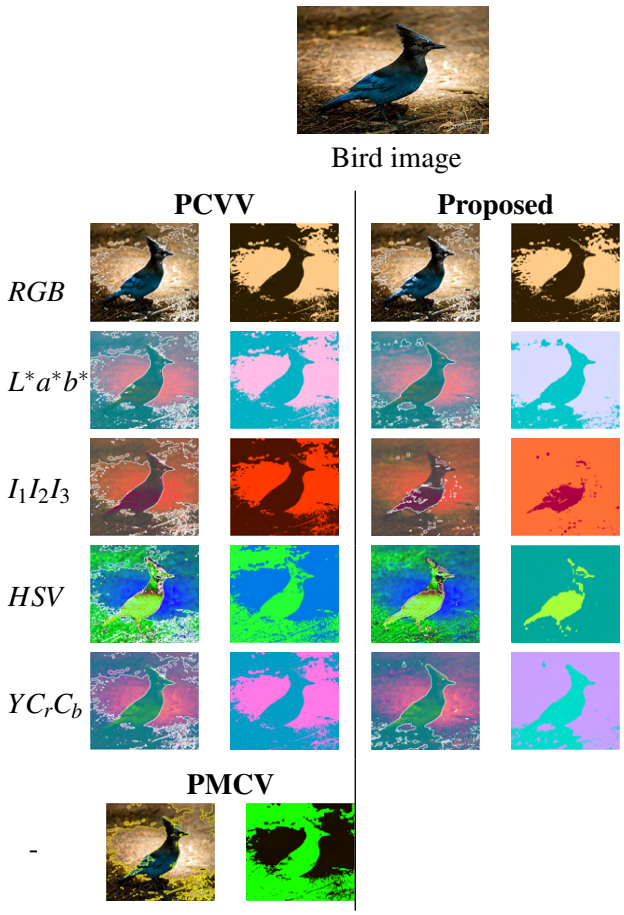

Fig. 6. *Segmentation results of the strong light uniform bird image in most used color spaces. Columns 2 and 3 show the converged zero level set function and corresponding segmented image by classic B-PCVV model, respectively. Columns 4 and 5 show the results by the proposed improved B-PCVV model. The last row shows the result of the PMCV model.*

Quantitative Evaluation in Bi-phase Case

Many datasets are used in these experiments:

–**Oxford 102 flowers dataset** (Nilsback and Zisserman, 2008): It consists of 8189 images divided into 102 flower species. The images were mostly collected from the web. We have selected 4 species consisting of 555 images that have their ground truth segmentation images available. That are: Berbeton Daisy (124 images), Geranium (223 images), Dahlia (109 images), and Imogen (99 images).

–**Butterfly dataset** (Wang *et al.*, 2009): It consists of 832 images for ten butterfly categories (55-100 images per category).

–**Caltech UCSD Birds 200-2011 dataset** (Welinder *et al.*, 2010): The images organized in sub-directories based on species. We have consider, in this evaluation, the first sub-directorie that regroups 60 images of Black Footed Albtross specie.

–**Weizmann dataset**(Alpert *et al.*, 2007): It is about 100 images collected from different sources.

–**Agronomic application datasets**: Three datasets are used: (i) **Weed/Crop** (Haug and Ostermann, 2015) that consists of 60 images of carrot crop. (ii) **Wheat 2011** (Guo *et al.*, 2017) contains 19 images of wheat crop acquired in a variety of outdoor light conditions, (iii) **Wheat 2012** is dataset with 17 images that reflect challenging light condition and background complexity (Guo *et al.*, 2017). The images represent top views of the crops. Resulting images reflect two regions (vegetation and soil) hereby, the processing with biphase level sets is very adequate given its ability to extract foreground from background.

The segmentation accuracy *Acc* and number of iterations obtained on these datasets are reported in Tab. 5. These results show that the proposed method improves the segmentation accuracy and the convergence rapidity in almost all datasets. Nevertheless, the degree of improvement varies among the datasets and the different color spaces.

Averagely, on oxford flowers dataset, our method improves the *Acc* of B-PCVV in $L^*a^*b^*$, $I_1I_2I_3$, and YC_rC_b, by 5.863%, 4.406% and 5.567%, respectively. Furthermore, the convergence is two iterations faster.

On Black Footed Albtross file of Caltech UCSD Birds dataset, Our method is ranked the first among all three models. A good accuracy gain is obtained. It is quantified to 10.955% in $L^*a^*b^*$, to 7.652% in $I_1I_2I_3$, and to 9.860% in YC_rC_b. In term of convergence rapidity, the proposed model achieves the convergence in less four iterations compared to B-PCVV.

Less accuracy gain is obtained on Butterfly datasets, where a many species of butterfly to be segmented present sub-regions with different colors. However, with the proposed method the *Acc* is slightly improved compared to B-PCVV by 3.624%, 5.494%, and 8.248% in in $L^*a^*b^*$, $I_1I_2I_3$, and YC_rC_b, respectively.

Generally, on Weizmann dataset the three models show lower performance. The best results are obtained by B-PCVV model. The proposed method is ranked the second. This can be explained by the fact that several images in this dataset present a complex background and intensity inhomogeneities. Consequently, segmentation using Chan-Vese bi-phase level set has limit performance.

On the above datasets, the proposed method produced similar and sometimes lower performance on

Table 4. *The obtained victor λ in the experiments on Figs 4, 5 and 6 for each considered color space*

Color spaces	Fig. 4: Horse	Fig. 5: Flower	Fig. 6 :Bird
RGB	[0.25, 0.28, 0.45]	[0.55, 0.25, 0.19]	[0.24, 0.13, 0.61]
$L^*a^*b^*$	[0.02, 0.41, 0.55]	[0.04, 0.46, 0.49]	[0.01, 0.80, 0.17]
$I_1I_2I_3$	[0.03, 0.56, 0.40]	[0.04, 0.43, 0.60]	[0.00, 0.01, 0.97]
HSV	[0.90, 0.05, 0.03]	[0.44, 0.21, 0.34]	[0.71, 0.24, 0.03]
YC_rC_b	[0.02, 0.56, 0.41]	[0.03, 0.77, 0.18]	[0.01, 0.45, 0.52]

RGB color space. While the low performance on *RGB* could be related to the non-separation between the chroma and the luminance components. Furthermore, the histogram's distribution of each channel are similar.

The more significant improvements of our method are obtained on the agronomic datasets. On Weed/Crop dataset the improvements are about 6.74% in RGB space, 14.98% in $L^*a^*b^*$, 42.79% in $I_1I_2I_3$ and 27.35% in YC_rC_b. In addition, in term of iteration numbers, the proposed algorithm requires an average of 10 iterations before convergence while the convergence of B-PCVV model is achieved after 16 iterations in average in $L^*a^*b^*$ space.

Generally, the PMCV model achieves a close results to B-PCVV in almost datasets. Its worst *Acc* is obtained on Butterfly dataset. The convergence of PMCV is much slower because the optimization is via gradient decent method.

Based on these results and analysis, the proposed model has obvious advantages over other two models, specially when image acquired in outdoor light conditions. With the proposed heuristic formula, each channel, in a given color spaces, is weighted differently, then contributes according to it in the energy functional.

Performance of proposed Bi-phase on Medical Images

Active contours have been widely used to segment a variety of medical images. In this experiment, we compare the performance of our method against that of PCVV and PMCV to detect melanoma lesions. Fig 7 shows the performance of those methods on a set of four dermoscopic images with different degrees of intensity uniformity. The segmentation accuracies are reported in Table 6. The original images and and the corresponding ground truths are represented in the first and second rows, respectively. The segmentation results, presented as obtained binary level set, are depicted in row 3 for PCVV, row four for PMCV and row 5 for our method. The results shows a high accuracy (above 97%) on all images and for all methods (see Table 6). We can notice that the accuracy slightly decreases with the increases of the image uniformity (cases of column three and four). This is probably due to the fact that PCVV model is based on constant approximation of image intensity, which limits its performance in the presence of intensity inhomogeneities.

PERFORMANCE AND EVALUATION IN MULTI-PHASE FRAMEWORK CASE

Advantages of multiphase against Bi-phase

Fig. 8 shows the segmentation results of the proposed method in B-phase and multi-phase level set framework. The first image contains four phases (white flower, pink flower, green flower leaves and background). The second image has seven regions.
In the Bi-phase level set case the model performs the foreground/background segmentation (see the first row of Figs. 8(a) and 8(b)).
In multi-phase level sets (n curves) framework, the model has better performance because it is able to subdivide the image domain into 2^n regions, thereby two curves extracts correctly the four regions present in the first image (see second row of Fig. 8(a)). However, in the case of second images (with seven regions) the model merges the regions with close colorimetric information (such as the pink and purple flowers in Fig. 8(b))

Qualitative Evaluation in Multi-phase framework

In this experiment, the proposed approach is tested on the two-horse image. It is expected to obtain 4 regions representing the sky, the black and brown horses and the background respectively. Fig. 9 shows the outcomes of the classic M-PCVV and the proposed model in different color spaces.
In the RGB color space both models perform identically, where they fail to extract correctly the four regions mentioned above. This is well observed in first column of Fig.9 where the brown horse and the ground are extracted as same region, while the sky is

Table 5. *Quantitative evaluations of the average segmentation accuracy Acc and number of iterations obtained on the above datasets*

Datasets (number of images)	Model	RGB	$L^*a^*b^*$	$I_1I_2I_3$	YC_rC_b
Oxford flowers (355)	B-PCVV	89.33/11	87.50/10	89.82/10	89.04/09
	Proposed	87.87/12	92.95/08	93.96/08	94.29/07
	PMCV		92.75/27		
Butterfly (832)	B-PCVV	67.40/17	72.85/16	67.77/17	67.52/17
	Proposed	67.48/17	75.59/15	71.71/16	73.59/16
	PMCV		57.53/65		
Caltech UCSD Birds 200-2011 (60 images)	B-PCVV	80.06/12	79.90/10	80.86/12	79.99/10
	Proposed	81.13/11	89.73/06	87.56/07	88.74/06
	PMCV		78.37/59		
Weizmann (100)	B-PCVV	74.17/12	75.11/12	73.51/12	74.11/12
	Proposed	73.30/11	73.11/12	72.39/10	73.17/11
	PMCV		73.60/87		
Weed/Crop (60)	B-PCVV	62.33/17	86.43/17	63.73/20	77.54/14
	Proposed	58.46/15	97.45/9	97.28/10	98.62/8
	PMCV		89.62/100		
Wheat2011 (19)	B-PCVV	63.50/19	68.41/18	63.50/19	67.87/15
	Proposed	62.98/19	94.53/10	94.29/13	94.60/10
	PMCV		69.87.62/98		
Wheat2012 (17)	B-PCVV	78.64/20	78.36/15	78.64/18	79.60/12
	Proposed	78.21/18	95.68/9	90.22/13	83.99/10
	PMCV		79.07/100		

subdivided to two regions (dark sky and clear sky). The best results are obtained by the proposed method in the $L^*a^*b^*$, $I_1I_2I_3$ and YC_rC_b color spaces where the four image's region are correctly extracted. However, in M-PCVV model the brown horse is regrouped with green ground.

Table 6. *Comparison of segmentation accuracy Acc(%) of the melanoma images in Fig.7*

	column 1	column 2	column 3	column 4
PCVV	97.38	99.17	99.51	98.85
PMCV	97.22	99.24	99.56	98.86
Proposed	97.56	99.47	99.01	98.86

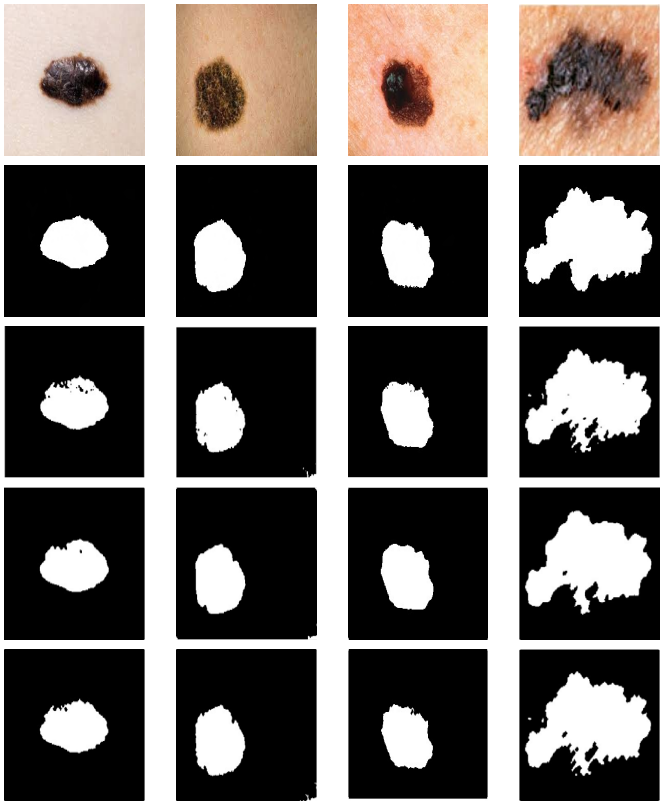

Fig. 7. *Segmentation results of four melanoma images with different inhomogeneous intensity. First row: original images. Second row: ground truth. The* 3^{rd} *to* 5^{th} *rows show the segmented images using PCVV, PMCV, and the proposed method, respectively.*

(a) Image with four regions

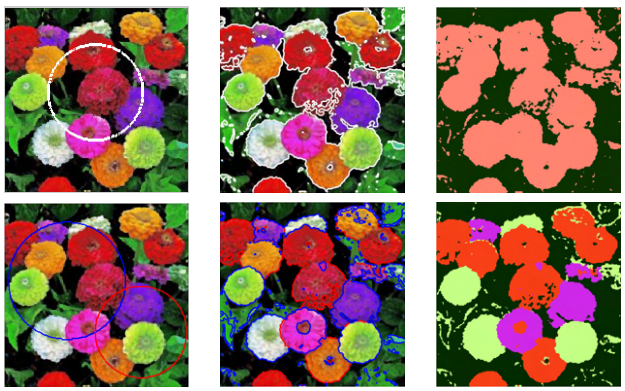

(b) Image with seven regions

Fig. 8. *Advantages of using multiphase level set to segment image more than two phases. For each subfigures: Top segmentation via biphase level set. Bottom segmentation via multiphase level sets.*

(a) Original image

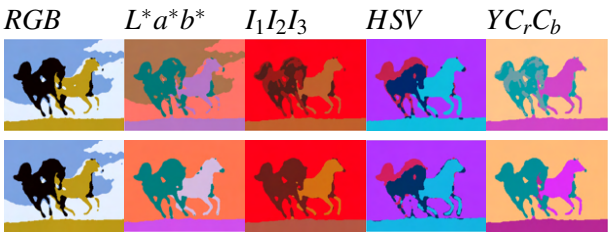

Fig. 9. *Segmentation of two-horses image by the classic M-PCVV model and the proposed one. The segmentation results are shown in different color spaces. The classic* $M-PCVV$ *in the second row and the proposed method in the third one.*

Performance of Multi-phase level sets in medical images

In this section we report the segmentation results obtained on Magnetic Resonance images of brain (healthy and affected with a tumor). Fig. 10 displays obtained results. The first column shows the original images with curves initialization (blue and red lines). The second column shows the convergence of the zero level sets Φ_1 and Φ_2 represented by the blue and red lines. The last column shows the segmented images where each region is represented by its mean intensity. The results show that the proposed model can successfully segment a healthy brain, where the three brain regions and background are extracted (see first row of 10). The brain lesion in the second image increases the number of regions to five, consequently, the proposed model extracted correctly the lesion and grouped brain regions with similar intensities (cerebro-spinal fluid and background) into the same segment.

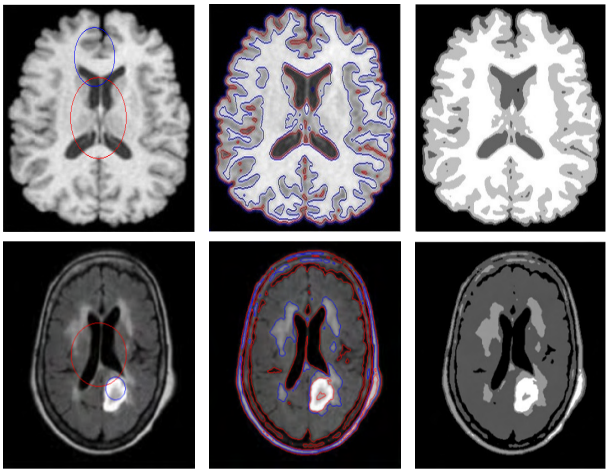

Fig. 10. *The proposed method segmentation results for brain MR images. The first column present original images with the initial zero level set functions (Φ_1 with blue line and Φ_2 with red line). The convergence of level set functions are shown on second column. The third column shows the four-phases segmented images*

DISCUSSION

Results of the experiments conducted on a variety of datasets (about 630 images) demonstrate the benefit of using an adaptive weighting that takes into account the color distribution of the image, since in almost all cases it outperformed the original PCVV method. The results also showed that the proposed approach does not improve the segmentation accuracy on RGB color space. Maybe this is because of the strong correlation that exists between the different channels of this color space.

The PMCV method performs well on most images but it seems that its performance deteriorates as the illumination becomes non-uniform (as shown in Fig. 6). Besides, PMCV requires larger memory space to store the channels of the two used color spaces.

The proposed approach deals very well with natural images even when the light conditions provide an uneven illumination, low contrast, saturated pixels, and similar problematic situations. Furthermore, it has good robustness to noise and level set initialization. Optimization via sweeping algorithm allows great saving in computing time compared to optimization via gradient decent. This gain is more important with the proposed contribution, where experiments reveal that our improvement of the PCVV accelerate the convergence especially when $L^*a^*b^*$, $I_1I_2I_3$ and YC_rC_b color spaces are used.

The variety of images which have been processed in the experiments confirm that there is no color space superior to all others in all types of images. Applying the proposed heuristic formula allows to get an optimum color space for a given image. For example the proposed approach on *HSV* color space gives the best result for segmenting "Bird image" (in Fig. 6), where the obtained optimum space is $[0.71 \times H, 0.24 \times S, 0.03 \times V]$ thus it highlights the Hue component and attenuates the illumination.

CONCLUSION

We have proposed an approach for foreground-background segmentation in color images. The main contribution of the proposed work consists of devising an automatic computation of the weight vector used by the energy functional of the active contours approach.

Our experiments showed that contrary to the PCVV model, our method is able to segment images in non-uniform lighting environment. They also showed that the optimization via sweeping principal speeds up the segmentation operation and reduces the number of parameters that require tuning.

We are presently working on the application of our method to other active contour models that may lead to better segmentation results on images with non-uniform intensity such as the Local-Global Region-based active contour family (Boutiche and Abdesselam, 2017). Finally, it can be worth to incorporate some color space features in the heuristic function and also exploring the possibility to learn the weights using machine learning.

REFERENCES

Alpert S, Galun M, Basri R, Brandt A (2007). Image segmentation by probabilistic bottom-up aggregation and cue integration. In: Proc. Cvpr. Ieee.

Boutiche Y, Abdesselam A (2017). Fast algorithm for hybrid region-based active contours optimisation. Iet Image Process 11:200–9.

Brox T, Rousson M, Deriche R, Weickert J (2010). Colour, texture, and motion in level set based segmentation and tracking. Image Vision Comput 28:376–90.

Burger W, Burge MJ (2009). Digital Image Processing. Springer-Verlag London.

Chan F, Lam F, Zhu H (1998). Adaptive thresholding by variational method. Ieee T Image Process 7:468–73.

Chan TF, Sandberg B, Vese LA (2000). Active contours without edges for vector-valued images. J Vis Commun Image R 11:130–41.

Dev S, Lee YH, Winkler S (2014). Systematic study of color spaces and components for the segmentation of sky/cloud images. In: Ieee Image Proc.

Garcîa-Lamont F, Cervantes J, Lopez-Chau A, Rodrîguez L (2018). Segmentation of images by color features: A survey. Neurocomputing 292:1–27.

García-Ugarriza L, Saber E, Amuso V, Shaw M, Bhaskar R (2008). Automatic color image segmentation by dynamic region growth and multimodal merging of color and texture information. In: ICASSP conference.

Gore JC, Ding Z, Li C, Kao C (2007). Implicit active contours driven by local binary fitting energy. In: Proc. Cvpr. Ieee.

Guo W, Zheng B, Duan T, Fukatsu T, Chapman S, Ninomiya S (2017). Easypcc: Benchmark datasets and tools for high-throughput measurement of the plant canopy coverage ratio under field conditions. Sensors 17.

Haug S, Ostermann J (2015). A crop/weed field image dataset for the evaluation of computer vision based precision agriculture tasks. In: Computer Vision - ECCV 2014 Workshops.

He L, Osher S (2007). A fast multiphase level set algorithm for solving the chan-vese model. Proc Appl Math 7:1041911–912.

Hernández-Hernández J, García-Mateos G, González-Esquiva J, Escarabajal-Henarejos D, Ruiz-Canales A, Molina-Martínez J (2016). Optimal color space selection method for plant/soil segmentation in agriculture. Comput Electron Agr 122:124–132.

Hoogi A, Subramaniam A, Veerapaneni R, Rubin DL (2017). Adaptive estimation of active contour parameters using convolutional neural networks and texture analysis. Ieee T Med Imaging 36:781–91.

Hu Q, Tian J, He DJ (2017). Wheat leaf lesion color image segmentation with improved multichannel selection based on the chan–vese model. Comput Electron Agr 135:260–8.

Kass M, Witkin AP, Terzopoulos D (1988). Snakes: Active contour models. Int J Comput Vis 1:321–31.

Lei Y, Weng G (2021). A robust hybrid active contour model based on pre-fitting bias field correction for fast image segmentation. Signal Process image Volume 97:116351.

Li C, Xu C, Gui C, Fox MD (2005). Level set evolution without re-initialization: A new variational formulation. In: Proc. Cvpr. Ieee, vol. 1. Washington, DC, USA: IEEE Computer Society.

Li C, Xu C, Gui C, Fox MD (2010). Distance regularized level set evolution and its application to image segmentation. Ieee T Image Process 19:3243–54.

Li X, Wang X, Dai Y (2018). Adaptive energy weight based active contour model for robust medical image segmentation. J Signal Process Sys 90:449–65.

Moallem P, Mousavi BS, Monadjemi SA (2011). A novel fuzzy rule base system for pose independent faces detection. Appl Soft Comput 11:1801–10.

Mousavi BS, Fazlollah S, Razmjooy N (2013). Color image segmentation using neuro-fuzzy system in a novel optimized color space. Neural Comput Appl 23:1513–20.

Mumford D, Shah J (1989). Optimal approximation by piecewise smooth function and associated variational problems. Lect Notes Pure Appl 42:577–685.

Nakib A, Oulhadj H, Siarry P (2007). Image histogram thresholding based on multiobjective optimization. Signal Process 87:2516–34.

Ng HF (2006). Automatic thresholding for defect detection. Pattern Recogn Lett 27:1644–49.

Nilsback ME, Zisserman A (2008). Automated flower classification over a large number of classes. In: 2008 Sixth Indian Conference on Computer Vision, Graphics Image Processing.

Song B, Chan T (2002). A fast algorithm for level set based optimization. CAM UCLA 68:02–68.

Subudhi P, Mukhopadhyay S (2021). A statistical active contour model for interactive clutter image segmentation using graph cut optimization. Signal Process 184:108056.

Vandenbroucke N, Macaire L, Postaire JG (2003a). Color image segmentation by pixel classification in an adapted hybrid color space. application to soccer image analysis. Comput Vis Image Und 90:190–216.

Vandenbroucke N, Macaire L, Postaireb J (2003b). Color image segmentation by pixel classification in an adapted hybrid color space. application to soccer image analysis. Comput Vis Image Und 90:190–216.

Vese LA, Chan TF (2002). A multiphase level set framework for image segmentation using the mumford and shah model. Int J Comput Vision 50:271–93.

Wang J, Markert K, Everingham M (2009). Learning models for object recognition from natural language descriptions.

Wang P, Hu X, Li Y, Liu Q, Zhu X (2016). Automatic cell nuclei segmentation and classification of breast cancer histopathology images. Signal Process 122:1–13.

Welinder P, Branson S, Mita T, Wah C, Schroff F, Belongie S, Perona P (2010). Caltech-UCSD Birds 200. Tech. Rep. CNS-TR-2010-001, California Institute of Technology.

Zhang X, Xiao P, Feng X, He G (2019). Another look on region merging procedure from seed region shift for high-resolution remote sensing image segmentation. Isprs J Photogramm 148:197–207.